01 Aug 2005

Comparison of Near-Field Millimeter-Wave Probes for Detecting Corrosion Precursor Pitting under Paint

Mohammad Tayeb Ahmad Ghasr
Missouri University of Science and Technology, mtg7w6@mst.edu

Sergey Kharkovsky
Missouri University of Science and Technology

R. Zoughi
Missouri University of Science and Technology, zoughi@mst.edu

Russell A. Austin

Recommended Citation

Comparison of Near-Field Millimeter-Wave Probes for Detecting Corrosion Precursor Pitting Under Paint

Mohammad Tayeb Ghasr, *Member, IEEE*, Sergey Kharkovsky, *Senior Member, IEEE*, Reza Zoughi, *Senior Member, IEEE*, and Russell Austin

Abstract—Aircraft structural components such as wings and fuselages are constantly exposed to harsh environments, which make them susceptible to corrosion initiation and growth. To complicate matters, corrosion is normally hidden under paint and primer and cannot be visually detected until significant corrosion has occurred, causing the paint to blister. Corrosion of this type is usually preceded by the presence of corrosion precursor pitting. Hence, early detection of pitting is a critical issue in the maintenance of an aircraft and its structural components. Near-field microwave nondestructive testing techniques have been successfully used for detection of corrosion under paint, including very small laser machined pits. However, it is desirable to improve the spatial resolution associated with these techniques so that pits with dimensions in the range of a few hundreds of micrometers can be effectively detected. In this paper, a comparison between several different millimeter-wave open-ended rectangular waveguide-based probes is made for the detection and evaluation of corrosion precursor pitting at Ka-band (26.5–40 GHz) and V-band (50–75 GHz). A number of laser machined pits with dimensions varying between 150 to 500 μm were produced for this investigation. Using these probes, millimeter-wave images of these pits were produced, indicating that the modified open-ended rectangular waveguide probes, namely, single and double tapered and dielectric slab-loaded waveguide probes, were successful in detecting small pits. The results of this investigation, along with a complete discussion of the results, are presented.

Index Terms—Corrosion, microwave imaging, millimeter wave, nondestructive testing, pitting.

I. BACKGROUND

CRITICAL aircraft structural components, such as wings and fuselages, are exposed to harsh environments that vary considerably in temperature and moisture content. These varied environmental conditions lead to corrosion of these components. In most cases the corrosion is hidden under paint and primer and cannot be visually detected. Thus, detection is only possible when corrosion becomes severe and causes blistering of the paint. When this happens, a relatively large area must be rehabilitated, which may require significant time, resources, and downtime of the aircraft. The initiation of corrosion is preceded by the presence of corrosion precursor pitting. Detection of precursor pitting yields information about the susceptibility to corrosion initiation [1]–[3]. The size (area and depth) of a precursor pitting is naturally very small (fractions of a millimeter); otherwise, when it becomes relatively large, the corrosion process has already initiated. Therefore, nondestructive detection of corrosion precursor pitting is extremely important and desirable for aircraft structural health monitoring and maintenance.

The small size of a pit and the fact that it is hidden under paint and primer limit the number of nondestructive testing (NDT) methods that can be used to detect it and evaluate its size. There are several NDT methods that may be used for this purpose. Although there are many standard NDT techniques available for a wide range of applications, there is no single technique that can be used for detecting small pits under paint [4]–[6]. Additionally, these techniques each have their own advantages and disadvantages when used for detecting corrosion (and pitting) under paint. On the other hand, near-field microwave NDT methods have been successfully used for detecting corrosion under thin and relatively thick dielectric coatings such as paint and composite materials [7]–[10]. Recently, near-field microwave NDT methods have also been successfully used for detecting corrosion precursor pitting in exposed as well as painted aluminum substrates [11], [12]. Near-field microwave NDT techniques, using different types of probes, such as open-ended rectangular waveguides, offer many advantages when inspecting complex composite structures [13].

1) Measurements can be conducted in contact as well as noncontact fashion, and when used in the latter mode, the distance between the probe and the composite under test, referred to as the standoff distance, may be optimized to increase measurement sensitivity.
2) Compared to the far-field or plane-wave approach, near-field approaches produce finer spatial resolutions, since spatial resolution in the near-field of a probe is primarily a function of the probe dimensions and not necessarily a function of wavelength. Near-field probes are usually relatively small; consequently, when used for millimeter-wave imaging (as will be explained later), they produce high spatial resolution images, which is very attractive for detecting very small pits.
3) There are several different types of near-field probes that may be used (open-ended rectangular and circular waveguides, open-ended coaxial lines, microstrip patches, cavity resonators, etc.), each providing its own unique advantageous features for a specific application.
4) There is no need for a bulky antenna. Near-field measurement systems are commonly small, handheld, portable, and operator friendly, and require low microwave power [13].

When operating in the near-field and for the purpose of microwave and millimeter-wave imaging, the electromagnetic properties (i.e., electric field distribution) and the aperture size of the probe significantly influence the resulting system spatial resolution and radiation efficiency. As mentioned earlier, open-ended rectangular waveguide probes have been successfully used to detect the presence of corrosion under paint and primer in both steel and aluminum substrates [7]–[10] and corrosion precursor pitting under paint [11], [12]. Near-field microwave NDT techniques with open-ended rectangular waveguide probes have also been used to detect other types of surface anomalies, such as scratches, cracks, and dents in metallic structures [14]–[18]. Standard open-ended rectangular waveguide probes have shown great promise for detecting precursor pitting larger than 500 μm in diameter (at frequencies higher than 30 GHz). However, for aircraft health monitoring and effective maintenance purposes, it is necessary to detect smaller pits since detection of smaller pits means the discovery of earlier corrosion initiation [11], [12]. Consequently, it is of great practical interest to increase the effective spatial resolution obtained by open-ended rectangular waveguide probes while maintaining a relatively high level of radiation efficiency (i.e., adequate signal radiation from the probe while reducing unwanted reflections due to mismatch between the probe and the waveguide). At a given operating frequency band, higher spatial resolution may be achieved by physically reducing the probe aperture dimensions through tapering the narrow and/or broad walls of the waveguide [11]. However, tapering the waveguide adversely affects the radiation efficiency of the probe and may cause significant unwanted reflections and less power radiated from it (depending on the taper geometry). Consequently, a tapered waveguide probe should be operated at small standoff distances and may become less sensitive to the presence of small pits under paint. Therefore, a compromise must be reached between higher spatial resolution and adequate probe radiation efficiency by electrically reducing the probe aperture size. It is well known that the dominant mode electric field inside a waveguide can be concentrated in a relatively small region by inserting a dielectric slab parallel to the narrow walls of the waveguide usually centered in the broad walls [19]–[21]. This modification to the dominant mode electric field distribution is equivalent to an effective (i.e., electrical) reduction in the waveguide broad dimension. Therefore, it is expected that such an open-ended dielectric slab-loaded waveguide probe would provide higher spatial resolution when used in the place of an ordinary open-ended waveguide of the same physical dimensions (e.g., the same frequency band) while maintaining higher radiation efficiency than a tapered waveguide probe.

To this end, modified versions of an open-ended rectangular waveguide probe, namely, single and double tapered and two different dielectric slab-loaded waveguide probes, were used to detect machined exposed and hidden (under thin dielectric coatings such as paint) pits. The influence of dielectric slab thickness and permittivity on the electric field distribution of the waveguide aperture was also numerically investigated. Finally, using two-dimensional (2-D) automated scanning tables and laboratory-designed reflectometers at Ka-band (26.5–40 GHz)
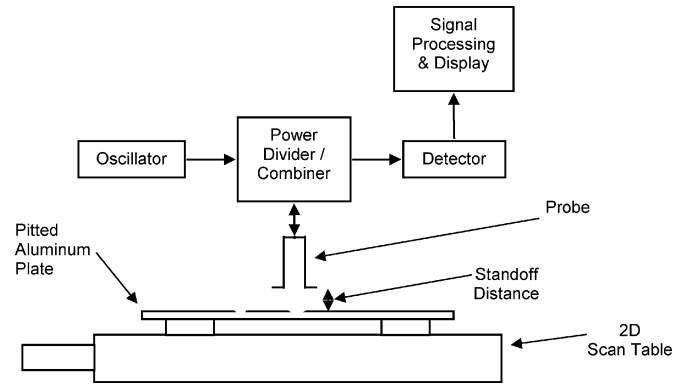

Fig. 1.   Laboratory setup.

and V-band (50–75 GHz), millimeter-wave images of pits of various sizes were produced. This paper presents the results of this investigation providing a comparison among these various modified near-field probes for detecting small corrosion precursor pitting.

II. APPROACH

Three sets of laser machined pits with openings (diameters) and depths ranging from 100 to 500 μm were produced on a 3-mm-thick aluminum plate. One set of pits was left exposed, while the other two sets were covered by a thin layer of paint and appliqué (paint-like polymer), respectively. Pits were spaced about 40 mm apart. The aluminum plate was placed on a 2-D automated scanning table capable of moving the plate in two directions at very small increments. The near-field millimeter-wave measurement systems or reflectometers were then fixed at a desired standoff distance above the plate, as shown in Fig. 1. A reflectometer consists of an oscillator (set a desired frequency), which feeds an open-ended probe via a signal divider/combiner. A portion of this signal is then supplied to the probe and becomes incident upon the pitted aluminum plate. Subsequently, the reflected signal from the plate is picked up by the probe and mixed with a portion of the transmitted signal (i.e., reference signal). This results in the difference between the phase and/or magnitude of these two signals and a signal proportional to their difference is fed into a display or indicator [13]. As the aluminum plate and the probe move with respect to each other (i.e., raster or C-scan), the reflected signal from the plate changes if an anomaly (i.e., a pit) is present. The change in the phase and/or magnitude of the reflected signal due to the pit indicates its presence and can be used to evaluate its dimensions. As the scanning table moves the plate under the probe, a 2-D matrix consisting of dc voltages proportional to the local reflection properties of the plate is produced. These voltages are then normalized (with respect to the highest value) in the data matrix, and different grayscale levels are assigned to them, resulting in a corresponding image of the scanned area. An image produced in this way provides information about relative signal variation in that image only, and the same two greyscale levels in two different images do not correspond to the same detected voltage values [13]. Therefore, in some cases when two images need to be compared, their matrices can be augmented first and then the new matrix is normalized and a new image is produced. In this
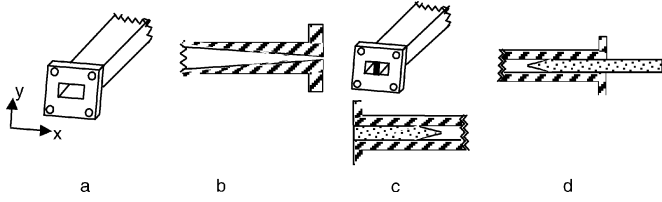
Fig. 2. Open-ended probes. (a) standard rectangular waveguide. (b) Tapered waveguide. (c) Dielectric slab-loaded waveguide. (d) Dielectric waveguide.

way, the voltage outputs in different regions of the original two images scan can be directly compared.

A small pit is not expected to strongly scatter the incident microwave or millimeter-wave signal. Consequently, when a microwave or millimeter-wave signal interacts with a pit and is finally picked up by the probe, the phase variation in the scattered signal is a stronger indication of the presence of the pit than the magnitude variation [13]. Therefore, throughout this investigation, phase-sensitive millimeter-wave reflectometers were utilized.

Finally, several open-ended probes were designed and developed for the purpose of this investigation operating at Ka-band (26.5–40 GHz) and V-band (50–75 GHz). These open-ended probes consisted of a) rectangular waveguides, b) single- and double-tapered rectangular waveguides, c) dielectric slab-loaded waveguides, and d) dielectric waveguides that are similar to the dielectric slab-loaded waveguides but with the dielectric slab extended out of the waveguide aperture. The schematics of these probes are shown in Fig. 2.

III. RESULTS

A. Simulation of Electric Field Distribution

As mentioned above, changing the aperture distribution of the electric field in a waveguide probe may affect the spatial resolution obtained by it when used for imaging. In a dielectric slab-loaded waveguide, the electric field tends to concentrate in the slab [19]–[21]. The dominant mode electric field distribution in a dielectric slab-loaded waveguide as a function of thickness and dielectric constant ($\varepsilon_r = \varepsilon_r' - j\varepsilon_r''$, where the real part is the relative to free-space permittivity and the imaginary part is the relative loss factor) of the slab was investigated numerically using the expressions found in [19].

Fig. 3 shows the calculated electric field distribution of the dominant TE_{10} mode in a Ka-band rectangular waveguide (WR-28) loaded with a 1-mm-thick dielectric slab (in the center of the waveguide broad dimension) for four different relative permittivity values of: 1) $\varepsilon_r' = 1$ (no dielectric slab), 2) $\varepsilon_r' = 2.5$, 3) $\varepsilon_r' = 4$, and 4) $\varepsilon_r' = 9.8$ (assuming lossless dielectric slabs for all cases, i.e., $\varepsilon_r'' = 0$). The results show that as the relative permittivity of the dielectric slab increases, the electric field becomes more concentrated within the dielectric slab. In addition, the electric field distribution in a dielectric slab-loaded waveguide depends on the width of the slab as well. Fig. 4 shows the normalized electric field distribution in a dielectric slab-loaded rectangular waveguide for a slab with $\varepsilon_r' = 9.8$ and normalized widths of $c/a = 0.05, 0.15$, and 0.3, respectively. In Fig. 4, c is the width of the dielectric slab
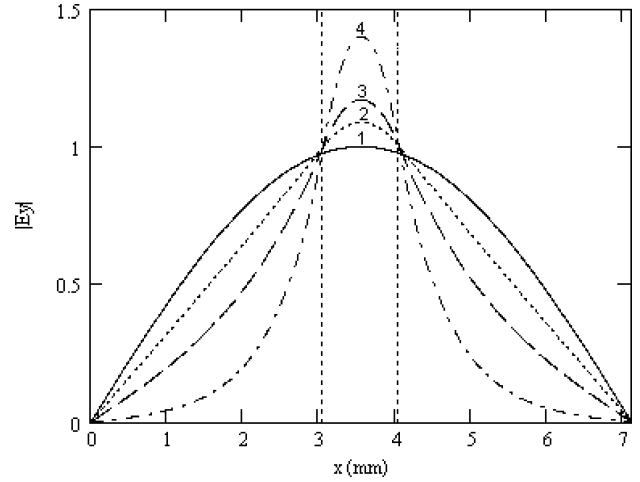

Fig. 3. TE_{10} mode electric field distribution in a rectangular waveguide loaded with a 1-mm-thick dielectric slab having various permittivities at 35 GHz: (1) $\varepsilon_r' = 1$, (2) $\varepsilon_r' = 2.5$, (3) $\varepsilon_r' = 4$, and (4) $\varepsilon_r' = 9.8$.
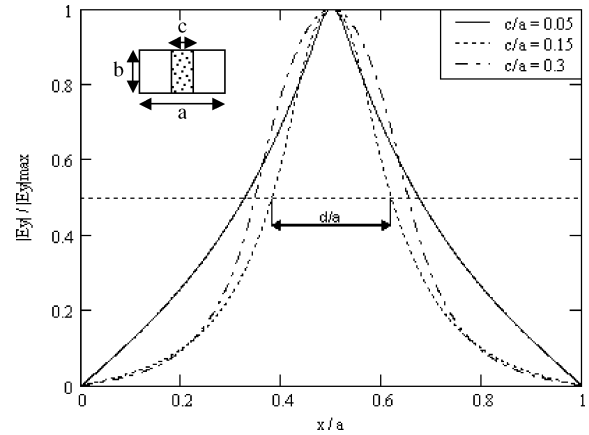

Fig. 4. Normalized TE_{10} mode electric field intensity distribution in a rectangular waveguide loaded with a dielectric slab with permittivity of $\varepsilon_r' = 9.8$ for different normalized slab width c/a.

and d is the extent of electric field concentration region at the selected level of $|Ey|/|Ey|_{\max} = 0.5$ (i.e., effective electric field localization).

It can be seen from Fig. 4 that for $\varepsilon_r' = 9.8$, d/a is not a monotonic function of normalized dielectric slab width. This fact is more clearly illustrated in Fig. 5, where d/a is plotted versus normalized dielectric slab thickness c/a for different relative permittivities of 1) $\varepsilon_r' = 2.5$, 2) $\varepsilon_r' = 4$, 3) $\varepsilon_r' = 9.8$, and 4) $\varepsilon_r' = 15$, respectively. The results show that for a given dielectric slab relative permittivity, there is an optimum slab width that gives the smallest effective extent of electric field localization which corresponds to the highest concentration of the electric field inside and near the slab. For example, when using a dielectric slab with relative permittivity of 9.8, the maximum localization of TE_{10} electric field occurs for a normalized slab width of approximately 0.13. Also, as expected, the optimum slab width decreases as the slab dielectric permittivity increases.

B. Imaging

1) Ka-Band Results: Previously it was shown that an open-ended rectangular waveguide probe and a double tapered probe
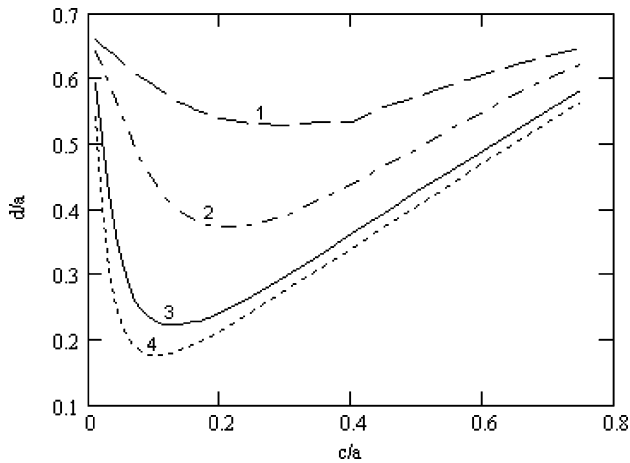
Fig. 5. The extent of normalized effective electric field localization d/a versus normalized slab width c/a for different dielectric permittivity of the slab: (1) $\varepsilon'_r = 2.5$, (2) $\varepsilon'_r = 4$, (3) $\varepsilon'_r = 9.8$, and (4) $\varepsilon'_r = 15$.

Fig. 6. Images of a pitting with a diameter of $\sim$ 1 mm and a depth of $\sim$ 1 mm obtained at a standoff distance of 1 mm using Ka-band probes. (a) Open-ended rectangular waveguide. (b) Dielectric slab-loaded rectangular waveguide. (c) Double-tapered Ka-band to U-band transition waveguide. (d) Single tapered waveguide.

at Ka-band were not capable of detecting machined pits smaller than 500 μm in diameter [11]. Therefore, in order to examine and compare the attributes of the various probes mentioned earlier, a pit with a diameter and a depth of approximately 1 mm was produced. This pit was scanned using four probes; namely, an open-ended rectangular waveguide (aperture dimensions of 7.11×3.56 mm), a double-tapered waveguide (aperture dimensions of 4.8×2.4 mm), a single-tapered waveguide (aperture dimensions of 7.11×0.5 mm), and a dielectric slab-loaded ($\varepsilon'_r = 9.8$ and $c/a = 0.14$) rectangular waveguide (aperture dimensions of 7.11×3.56 mm). The pit was scanned at a standoff distance of 1 mm for all cases, and the resulting images are shown in Fig. 6. In all of the images presented in this paper, the probes are oriented such that the broad dimension of the aperture is parallel to the vertical axes of the images (i.e., the electric field vector is parallel to the horizontal axes of the images). The dimensions shown in all images are in millimeters.

From Fig. 6, it is clear that each probe produced an image of the pit with a unique set of characteristics and features. The pit image produced by the open-ended waveguide probe consisted of two distinct spots, as shown in Fig. 6(a). This is primarily due to the fact that the pit dimension is much smaller than the waveguide aperture dimensions, resulting in two distinct interactions between the pit and the two edges of the waveguide aperture (i.e., corresponding to the board walls of the waveguide aperture). This type of interaction has also been observed when scanning a surface breaking crack in conducting plates [15]–[17]. This interaction becomes less significant as the standoff distance increases, resulting in a single spot indicating the pit [17]. This is an important issue, from the detection point of view, in that when detecting two spots, one is less likely to miss the pit. However, for smaller aperture dimensions, one is expected to detect one spot but with higher signal intensity. This is indicated by the images produced using the remaining probes, as both tapered waveguide probes and the dielectric slab-loaded waveguide probe produced one spot indicating the presence of the pit, as shown in Fig. 6(b)–(d). Moreover, the single tapered waveguide probe, which has the smallest narrow wall dimen-
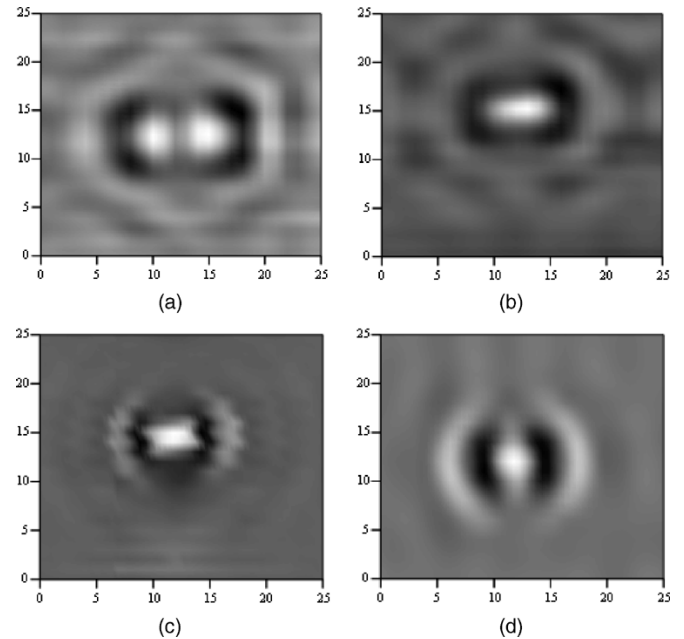
sion, produced an image very similar in shape to that of the actual pit [Fig. 6(d)].

Each image in Fig. 6 also shows rings around the image of the pit as a result of the standing wave set up between the waveguide flanges and the plate. Thus, the presence of the pit is depicted by these characteristic rings, which results in a more robust detection of a pit (i.e., higher probability of detection). Also, it is worth noting that the dielectric slab reduced the intensity of the rings, as expected (i.e., the electric field is concentrated at the center of the probe), as shown in Fig. 6(b).

The signal intensity associated with the pit in each image depends on the radiation efficiency of the particular probe used and the relative concentration of the electric field at its aperture. The images shown in Fig. 6 are individually normalized (as explained earlier), and therefore it is not possible to compare the difference in intensity between the images. However, when these images were augmented together before normalization (not shown in this paper), we observed that the double tapered and the dielectric slab-loaded waveguides produce images with higher contrast than the open-ended waveguide and the tapered waveguide. The double tapered waveguide has aperture dimensions that are smaller than the open-ended waveguide (i.e., field is concentrated in a smaller area). However, this dimension is not very small compared to the single tapered waveguide. Therefore, the radiation efficiency associated with the double tapered waveguide is not significantly less than that of the open-ended waveguide but higher than that of the single-tapered waveguide. The dielectric slab-loaded waveguide produces concentrated field along the broad walls of the waveguide aperture while maintaining adequate radiation efficiency.

On the contrary, obtaining finer spatial resolution by decreasing probe aperture dimensions results in a decrease in its
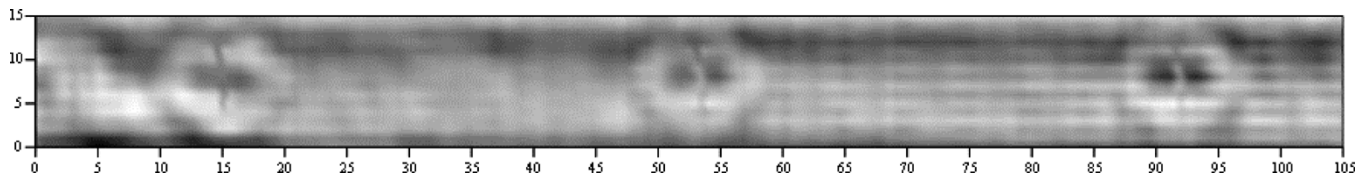
Fig. 7. Image of three pits of 500 μm in diameter and depths of (from left to right) 150, 200, and 500 μm, obtained using the single tapered probe at Ka-band.

radiation efficiency. Thus, since the radiation efficiency suffers in this case, measurements should be performed at a very small standoff distances. This is apparent in the results obtained using the single-tapered waveguide probe, which has been capable of detecting exposed machined pits of 500 μm diameter and depths as small as 150 μm. This corresponds to a relatively high spatial resolution while operating at a relatively low frequency. This is possible since the narrow wall dimension of this probe is comparable to the pit size. Fig. 7 shows the image of three 500-μm-diameter pits, each with depths of (from left to right) 150, 200, and 500 μm, respectively, obtained using the single tapered probe. In this image, the difference in the intensity of the indications corresponds to the variation in pit depth. This image was obtained at a standoff distance of less than a millimeter. For such small standoff distances, the probe output voltage is sensitive to variations in standoff distance. The original image was masked by the signal due to standoff distance variation. Consequently, the image was processed to remove the effect of variations in standoff distance.

Another promising probe for detecting small pits, especially under paint, is the dielectric waveguide probe. For this probe, the electric field is concentrated within the slab which is narrower than the waveguide it extends out of. Additionally, there is no waveguide flange in this case (i.e., no rings are expected around the image of a pit). Therefore, this probe is expected to produce higher spatial resolution images than the open-ended waveguide and the slab-loaded waveguide probes. Fig. 8 shows the image of a 500-μm-diameter and 150-μm-depth pit under paint obtained using a dielectric waveguide (aperture 3 × 1 mm) at a standoff distance of 0.2 mm. In this image, two spots indicating the pit are clearly visible since the pit diameter is smaller than the dielectric waveguide dimensions and the standoff distance is very small. These spots are created due to the interaction between the edge of the dielectric waveguide and the pit, as explained earlier. This is confirmed by measuring the distance between the centers of these spots, which is 3 mm and very close to the width of the dielectric waveguide. The results obtained using this dielectric waveguide could not be obtained using the other probes at Ka-band with the exception of the single-tapered probe, as shown in Fig. 7. It is important to note that both of these probes were capable of detecting micrometer-size pits only at very small standoff distances.

2) V-Band Probes: In order to increase the spatial resolution while maintaining high radiation efficiency, the frequency of operation may be increased. As the operating frequency increases, the physical aperture dimensions of the probe become smaller, resulting in higher spatial resolution. Fig. 9 shows three images of a 500-μm-diameter and 150-μm-depth pit under paint at a standoff distance of 0.5 mm obtained at V-band using a) an open-ended rectangular waveguide

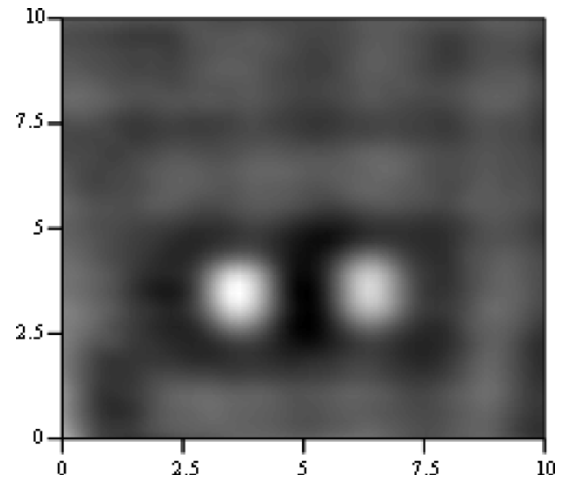Fig. 8. Image of a pit of 150 μm depth and 500 μm diameter under paint obtained using a dielectric waveguide probe at Ka-band.

(aperture dimensions of 3.8 × 1.9 mm), b) a double-tapered waveguide probe (aperture dimensions of 3.1 × 1.5 mm), and c) a double-tapered waveguide probe (aperture dimensions of 2.54 × 1.27 mm). By comparing the results, it is clear that the double tapered probe produced better image contrast than the open-ended rectangular waveguide probe. On the other hand, the open-ended rectangular waveguide [Fig. 9(a)] produced the more pronounced characteristics rings. This is primarily due to the fact that stronger standing waves are set up between the metal plate and the flange of the waveguide probe since this probe radiates more efficiently than the other two. As explained earlier, this is an advantageous feature from a detection point of view; however, this probe produces images with coarser spatial resolution than the other two. The best of these three probes, in terms of resolution at V-band, was to the smallest double tapered probe which was capable of detecting pits as small as 200 μm in diameter and a depth of 500 μm under paint and appliqué and pits as small as 150 μm in diameter and a depth of 500 μm when exposed.

Fig. 10 shows two images of a set of three pits with a diameter of 500 μm and depths of (from left to right) 150, 200, and 500 μm under paint and appliqué, respectively. These images were also obtained at a standoff distance of 0.5 mm. In these images, vertical lines are visible throughout the image with constant spacing of approximately 2 mm, corresponding to the half-wavelength at that frequency (70 GHz). These lines are due to standing surface waves formed on the sample due to reflections from the edge of the sample. The variation in the background signal level in Fig. 10(a) is due to the nonuniformity associated with the paint thickness. This is an issue to be considered since these variations may mask signals from smaller
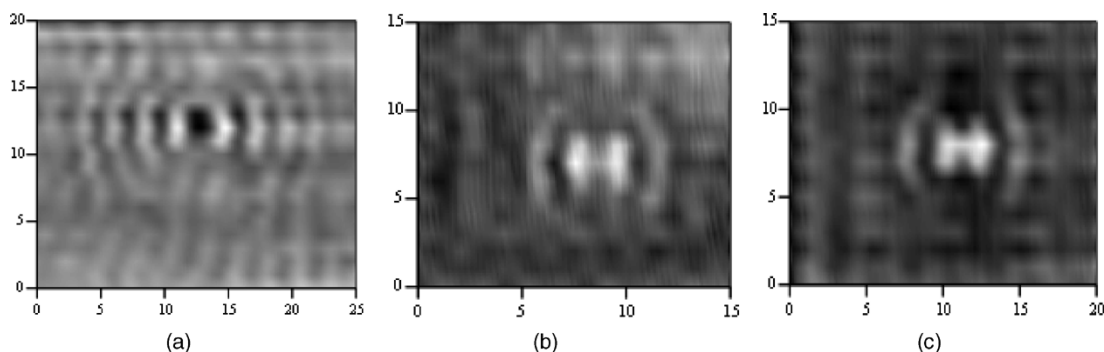
Fig. 9.　Images of a pit of 150 μm depth and 500 μm diameter under paint at a standoff distance of 0.5 mm using V-band probes. (a) Open-ended rectangular waveguide. (b) Double-tapered V-band to E-band transition waveguide probe. (c) Double-tapered V-band to W-band transition waveguide probe.
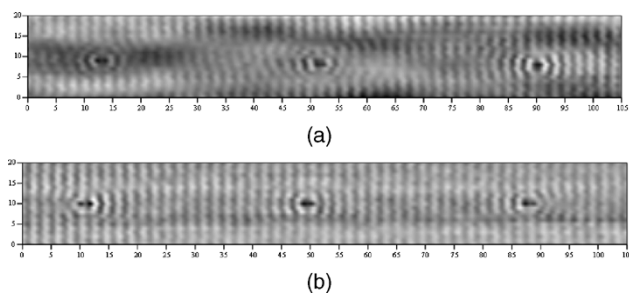

Fig. 10.　Image of three pits of 500 μm diameter and depths of (from left to right) 150, 200, and 500 μm, obtained at a standoff distance of 0.5 mm using an open-ended rectangular waveguide at V-band: (a) under paint and (b) under appliqué.

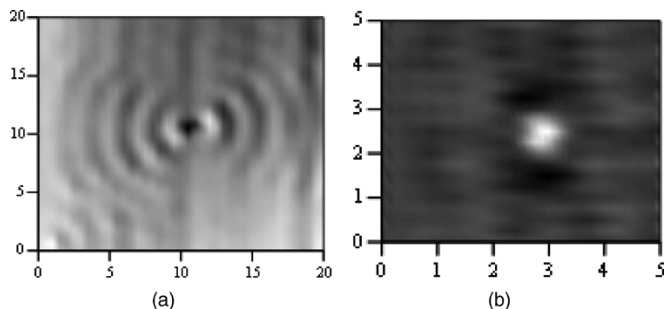Fig. 11.　Image of a pit of 200 μm depth and 500 μm diameter under paint obtained at a standoff distance of 0.5 mm at V-band using (a) dielectric slab-loaded waveguide probe and (b) dielectric waveguide probe.

pits. In contrast, the image in Fig. 10(b) is more uniform since the appliqué is more uniform in thickness than paint.

A dielectric slab-loaded waveguide at V-band produced images similar in characteristics to those at Ka-band except with higher resolution. For example, at a standoff distance of 0.5 mm, the dielectric slab-loaded waveguide at V-band produced an image [Fig. 11(a)] of the pit with a diameter of 500 μm and a depth of 200 μm with higher signal intensity corresponding to the spot in the image representing the pit and with reduced ring effects. Images at this frequency band are more suitable for pit size evaluation and shape determination. The probe that provided the best spatial resolution and image contrast was the dielectric waveguide probe at V-band. Fig. 11(b) shows the image of the same pit [as shown in Fig. 11(a), at V-band and a standoff distance of 0.5 mm, but using a dielectric waveguide

probe aperture with dimensions of approximately 1×1 mm]. This high-contrast image shows a single spot representing the pit with no rings. The dielectric waveguide probe was also used at higher standoff distances of up to 2 mm, at which point it was no longer capable of detecting the 500-μm-diameter pits. At smaller standoff distances, this probe was able to detect pits with sizes as small as 150 μm in diameter and 150 μm in depth. This is expected since this type of dielectric waveguide is not an efficient radiator compared to an open-ended rectangular waveguide. Due to its high resolution, the dielectric waveguide probe produces images that correspond more closely to the actual shape of a pit.

IV. CONCLUSION

Different types of near-field millimeter-wave probes for detection and evaluation of corrosion precursor pitting under paint using raster scanning were investigated and compared. The probes investigated produced images of a pit that depend on the type of the probe, relative aperture size of the probe and the pit, operating frequency, and standoff distance. At selected frequency bands, various pit dimensions, and range of standoff distances, the open-ended waveguide probe produced a double image of the pit as a signature of the probe aperture and distinct rings around the image as a signature of the probe flange. This type of image may provide high probability of detection, but for the evaluation of pitting, an image similar to the real shape of the pit is more desirable. A single pit image was obtained by a dielectric slab-loaded waveguide, dielectric waveguide probe, and tapered waveguide probe. It was shown that a significant increase in the electric field concentration may be obtained in a dielectric slab-loaded waveguide, and further concentration of the electromagnetic field can be accomplished in a dielectric waveguide.

The dielectric slab-loaded waveguide and dielectric waveguide probes provided a high level of detection sensitivity and relatively high spatial resolution, both increasing with the increase in the operating frequency. The tapered waveguide probe provided the highest resolution among all probes, but its detection sensitivity was lower than the dielectric slab-loaded waveguide probe. The dielectric waveguide probe produces images of high contrast and spatial resolution, which may be helpful in the evaluation and sizing of a pit.

One other issue to be considered is the physical strength of the probe and its rigidity, which favors the metallic waveguides more than the dielectric ones. In this case, tapering the waveguide may be the best solution to increase spatial resolution.

For measurements conducted in this investigation, the dielectric waveguide probe at V-band provided the optimal combination of spatial resolution and sensitivity for the detection and evaluation of pits under paint. The tapered waveguide probe may also be useful for pit detection and evaluation in cases of small standoff distances, such as when scanning exposed metal surfaces.

One of the issues that need to be overcome is the effect of standoff distance variation on the results. High-resolution probes are sensitive to standoff distance variation, which may mask the indication of a pit. Further processing may be required to "clean" such images and extract the indication of a pit.

REFERENCES

[1] R. Baboian, Ed., *Corrosion Tests and Standards: Application and Interpretation*. Philadelphia, PA: American Society for Testing and Materials, 1995.

[2] W. Funke, "Blistering of paint films," in *Corrosion Control by Organic Coatings*, H. Leidheiser Jr., Ed. Houston, TX: National Association of Corrosion Engineers, 1981, pp. 97–102.

[3] J. A. Collins, *Failure of Materials in Mechanical Design*, 2nd ed. New York: Wiley Interscience, 1993.

[4] V. S. Cecco, G. Van Drunen, and F. L. Sharp, "Eddy current manual," Chalk River Laboratories, AECL Rep. AECL-7523, vol. 1, 1983.

[5] S. Hansen, B. Mossawir, A. Ergun, F. Degertekin, and B. Khuri-Yakub, "Air-coupled nondestructive evaluation using micromachined ultrasonic transducers," in *IEEE Ultrasonic Symp.*, vol. 2, Oct. 1999, pp. 1037–1040.

[6] X. Han, L. Favro, L. Li, Z. Ouyang, G. Sun, R. Thomas, and D. Ashbaugh, "Quantitative thermal wave corrosion measurements on a DC-9 belly skin in the irregular paint thickness variations," in *Review of Progress in Quantitative Evaluation*, D. Thompson and D. Chimenti, Eds. Melville, NY: American Institute of Physics, 2000, vol. 20A, pp. 483–486.

[7] W. C. Fitzgerald, M. N. Davis, J. L. Blackshire, J. F. Maguire, and D. B. Mast, "Evanescent microwave sensor scanning for detection of subcoating corrosion," *J. Corrosion Sci. Eng.*, vol. 3, 2001. Paper no. 15.

[8] N. Qaddoumi, A. Shroyer, and R. Zoughi, "Microwave detection of rust under paint and composite laminates," *Res. Nondestructive Eval.*, vol. 9, no. 4, pp. 201–212, 1997.

[9] N. Qaddoumi, L. Handjojo, T. Bigelow, J. Easter, A. Bray, and R. Zoughi, "Microwave corrosion detection using open-ended rectangular waveguide sensors," *Mater. Eval.*, vol. 58, no. 2, pp. 178–184, Feb. 2000.

[10] D. Hughes, N. Wang, T. Case, K. Donnell, R. Zoughi, R. Austin, and M. Novack, "Microwave nondestructive detection of corrosion under thin paint and primer in aluminum panels," *Subsurface Sensing Technol. Applicat. (Special Issue on Advances and Applications in Microwave and Millimeter Wave Nondestructive Evaluation)*, vol. 2, no. 4, pp. 435–451, 2001.

[11] D. Hughes, R. Zoughi, R. Austin, N. Wood, and R. Engelbart, "Near-field microwave detection of corrosion precursor pitting under thin dielectric coatings in metallic substrates," in *Proc. 29th Annu. Rev. Progress Quantitative Nondestructive Evaluation*, vol. 22B, Bellingham, WA, Jul. 14–19, 2002, pp. 462–469.

[12] M. Ghasr, S. Kharkovsky, R. Zoughi, and R. Austin, "Comparison of near-field millimeter wave probes for detecting corrosion pit under paint," in *Proc. IEEE Instrumentation Measurement Technology Conf. (IMTC)*, Como, Italy, May 18–20, 2004, pp. 2240–2244.

[13] R. Zoughi, *Microwave Non-Destructive Testing and Evaluation*. Amsterdam, The Netherlands: Kluwer, 2000.

[14] R. Zoughi, C. Huber, S. Ganchev, R. Mirshahi, V. Otashevich, E. Ranu, and T. Johnson, "Rolled steel surface inspection using microwave methods," in *Proc. 8th Int. Symp. Nondestructive Characterization Materials*, vol. VIII, Boulder, CO, Jun. 15–20, 1997, pp. 285–290.

[15] C. Yeh and R. Zoughi, "A novel microwave method for detection of long surface cracks in metals," *IEEE Trans. Instrum. Meas.*, vol. 43, no. 5, pp. 719–725, Oct. 1994.

[16] C. Huber, H. Abiri, S. Ganchev, and R. Zoughi, "Analysis of the crack characteristic signal using a generalized scattering matrix representation," *IEEE Trans. Microw. Theory Tech.*, vol. 45, no. 4, pp. 477–484, Apr. 1997.

[17] ——, "Modeling of surface hairline crack detection in metals under coatings using open-ended rectangular waveguides," *IEEE Trans. Microw. Theory Tech.*, vol. 45, no. 11, pp. 2049–2057, Nov. 1997.

[18] R. Zoughi, C. Huber, N. Qaddoumi, E. Ranu, V. Otashevich, R. Mirshahi, S. Ganchev, and T. Johnson, "Real-time and on-line microwave inspection of surface defects in rolled steel," in *Proc. Asia-Pacific Microwave Conf. (APMC)*, Hong Kong, Dec. 2–5, 1997, pp. 1081–1084.

[19] L. Outifa, M. Delmotte, and H. Jullien, "Dielectric and geometric dependence of electric field and power distribution in a waveguide heterogeneously filled with lossy dielectrics," *IEEE Trans. Microw. Theory Tech.*, vol. 45, no. 8, pp. 1154–1161, Aug. 1997.

[20] N. Eberhardt, "Propagation in the off center E-plane dielectric loaded waveguide," *IEEE Trans. Microw. Theory Tech.*, vol. MTT-15, no. 5, pp. 282–289, May 1967.

[21] P. Vartanian, W. Ayres, and A. Helgesson, "Propagation in dielectric slab loaded rectangular waveguide," *IEEE Trans. Microw. Theory Tech.*, vol. MTT-6, no. 4, pp. 215–222, Apr. 1958.

Mohammad Tayeb Ghasr (M'04) received the B.S.E.E. degree from the American University of Sharjah, UAE, in 2002 and the M.S. degree in electrical and computer engineering from the University of Missouri-Rolla (UMR) in 2004.

Since 2000, he has been a Graduate Research Assistant with the Applied Microwave Nondestructive Testing Laboratory, Electrical and Computer Engineering Department, UMR. His current research involves the detection of corrosion under paint and corrosion precursor pitting in aircraft structures using microwave and millimeter-wave nondestructive testing techniques.

Sergey Kharkovsky (M'01–SM'03) was born in Mayskiy, Caucasus region, Russia, in 1952. He received the electronics engineering degree from Kharkov Institute of Radioelectronics, Kharkov, Ukraine, in 1975, the Ph.D. degree from Kharkov State University, Kharkov, in 1985, and the D.Sc. degree from the Institute of Radio-Physics and Electronics (IRE), National Academy of Sciences of Ukraine, Kharkov, in 1994, both in radiophysics.

From 1975 to 1998, he was a Member of the Research Staff with IRE. From 1998 to 2002, he was a Professor in the Electrical and Electronics Engineering Department, Cukurova University, Adana, Turkey. His research area with IRE was developing and investigating a new millimeter-wave technique, including dielectric resonators with whispering gallery modes and solid-state oscillators, and its application for material characterization. He is now a Visiting Associate Professor in the Electrical and Computer Engineering Department, University of Missouri-Rolla. His current research interest is nondestructive testing and evaluation of composite structures using microwaves and millimeter waves.

Reza Zoughi (S'85–M'86–SM'93) received the B.S.E.E., M.S.E.E., and Ph.D. degrees in electrical engineering (radar remote sensing, radar systems, and microwaves) from the University of Kansas, Lawrence.

From 1981 to 1987, he was with the Radar Systems and Remote Sensing Laboratory (RSL). Currently, he is the Schlumberger Distinguished Professor of Electrical and Computer Engineering at the University of Missouri-Rolla (UMR). From 1987 to 2001, he was with the Electrical and Computer Engineering Department, Colorado State University (CSU), where he was a Professor and established the Applied Microwave Nondestructive Testing Laboratory. His current areas of research include developing new nondestructive techniques for microwave and millimeter-wave inspection and testing of materials, developing new electromagnetic probes to measure characteristic properties of material at microwave frequencies, and developing embedded modulated scattering techniques for NDT purposes, in particular for complex composite structures. He was the Business Challenge Endowed Professor of Electrical and Computer Engineering while at CSU. He is the author or coauthor of more than 300 journal publications, conference proceedings and presentations, technical reports, and overview articles. He is also the author of *Microwave Nondestructive Testing and Evaluation Principles* (Norwell, MA: Kluwer Academic, 2000) and the coauthor (with A. Bahr and N. Qaddoumi) of a chapter on "Microwave Techniques" in *Nondestructive Evaluation: Theory, Techniques, and Applications* (New York: Marcel Dekker, 2002). He has received seven patents in the field of microwave nondestructive testing and evaluation. He is an Associate Technical Editor for *Research in Nondestructive Evaluation* and *Materials Evaluation*. He was the Guest Associate Editor for the Special Microwave NDE Issue of *Research in Nondestructive Evaluation* and Co-Guest Editor for the Special Issue of *Subsurface Sensing Technologies and Applications: Advances and Applications in Microwave and Millimeter Wave Nondestructive Evaluation*. He was the Research Symposium Co-Chair for the ASNT Spring Conference and 11th Annual Research Symposium in March 2002 in Portland, OR.

Dr. Zoughi is a Member of Sigma Xi, Eta Kappa Nu, and the American Society for Nondestructive Testing. He has received two Outstanding Teaching Commendations, an Outstanding Teaching Award, and the Dean of Engineering Excellence in Teaching Award from UMR. He was voted the most outstanding teaching faculty seven times by the junior and senior students in the Electrical and Computer Engineering Department, CSU. He received the College of Engineering Abell Faculty Teaching Award in 1995. He is the 1996 recipient of the Colorado State Board of Agriculture Excellence in Undergraduate Teaching Award. He was recognized as an honored researcher for seven years by the Colorado State University Research Foundation. He has given numerous invited talks on the subject of microwave nondestructive testing and evaluation. He is an Associate Technical Editor for the IEEE TRANSACTIONS ON INSTRUMENTATION AND MEASUREMENT. He was Technical Chair for the IEEE Instrumentation and Measurement Technology Conference (IMTC2003) in Vail, CO. He was Guest Editor for the IMTC2003 Special Issue of the IEEE TRANSACTIONS ON INSTRUMENTATION AND MEASUREMENT. He is a member of the Administrative Committee of the IEEE Instrumentation and Measurement Society (2005–2008).

Russell Austin received the B.S. degree in materials engineering from the New Mexico Institute of Mining and Technology, Socorro.

He is the NDT Division Head with Texas Research Institute Austin, Inc., where he has worked since 1993. Previously, he spent two years with the NDT group at Argonne National Laboratories. He has written numerous papers, co-authored two books, and has two patents pending. His primary research areas are ultrasonic, acoustic emission, and microwave NDT. He is also involved in embedded systems for continuous health monitoring of structures and aircraft.